Mechanisms Forcing an Antarctic Dipole in Simulated Sea Ice and Surface Ocean Conditions

Marika Holland
National Center for Atmospheric Research
PO Box 3000
Boulder, CO 80307
Phone: 303-497-1734
Fax: 303-497-1700
mholland@ucar.edu

Cecilia Bitz
Polar Science Center
Applied Physics Laboratory
1013 NE 40th St.
Seattle WA 98105 USA

and

Elizabeth Hunke
T-3 Fluid Dynamics Group
MS-B216
Los Alamos National Laboratory
Los Alamos, NM 87545

Submitted to: Journal of Climate, April 13, 2004

Revised, October, 2004

Abstract

The mechanisms forcing variability in southern ocean sea ice and sea surface temperature from 600 years of a control climate coupled model integration are discussed. As in the observations, the leading mode of simulated variability exhibits a dipole pattern with positive anomalies in the Pacific sector associated with negative anomalies in the Atlantic. We find that in the Pacific, ocean circulation changes associated with variable wind forcing modify the ocean heat flux convergence and sea ice transport, resulting in sea surface temperature and sea ice anomalies. The Pacific ice and ocean anomalies persist over a number of years due to reductions in ocean shortwave absorption reinforcing the initial anomalies. In the Atlantic sector, no single process dominates in forcing the anomalies. Instead there are contributions from changing ocean and sea ice circulation and surface heat fluxes. While the absorbed solar radiation in the Atlantic is modified by the changing surface albedo, the anomalies are much shorter-lived than in the Pacific because the ocean circulation transports them northward, removing them from ice formation regions. Sea ice and ocean anomalies associated with the El Nino-Southern Oscillation and the Southern Annular Mode both exhibit a dipole pattern and contribute to the leading mode of ice and ocean variability.

1. Introduction

The southern ocean is characterized by large variability with considerable low frequency content. This is due to the unique properties of this region, including considerable deep and intermediate water formation, which allows for increased ocean heat uptake, and an interacting sea ice cover, which modifies the surface albedo and ice-ocean-atmosphere heat exchange. The water mass formation that occurs in this region provides important links to the global ocean circulation, allowing variability in the southern ocean to affect global climate conditions. Additionally, the Antarctic Circumpolar Current (ACC) system acts as the only direct link connecting the worlds major ocean basins, allowing for signals to be transmitted directly among these basins.

There have been a number of observational studies that examine coupled variability in the southern ocean. Many of these fall into two different, but related, categories: Antarctic circumpolar wave (ACW) studies (White and Peterson, 1996) and Antarctic Dipole studies (Yuan and Martinson, 2000). The ACW phenomena is seen in southern hemisphere sea surface temperature (SST), atmospheric sea level pressure (SLP), meridional wind stress, ice edge extent anomalies, and sea surface height anomalies (e.g. White and Peterson, 1996; Jacobs and Mitchell, 1996). These covarying anomalies exhibit a zonal wavenumber-2 structure and propagate eastward at a speed of roughly 8 cm/s, taking 8-10 years to circle the globe. However, as discussed by Connolley (2003), in examining data from 1968-1999, the ACW is only clearly evident from 1985-1994. Before and perhaps after this, the signal,

particularly in SLP, has a different spatial structure (wave-3) and does not clearly propagate.

Climate model simulations have been able to simulate ACW-like variability (e.g. Christoph et al, 1998; Cai et al., 1999; Haarsma et al., 2000), in that they obtain SST anomalies that propogate eastward in connection with the Antarctic circumpolar current. However, these studies generally do not exhibit phase locking between the ocean and atmospheric anomalies. Instead, they simulate a standing atmospheric wave in SLP, which often exhibits a zonal wavenumber 3 pattern, overlying a propagating ocean signal. The SSTs are typically driven by anomalous surface heat fluxes and their importance in driving changes in the atmospheric conditions differs between the different studies. In some studies (Christoph et al., 1998), the SST anomalies are strongest in the Pacific (as observed) and strongly dissipate in the Atlantic and Indian sectors making it unclear whether they propagate entirely around the continent. Many details of the structure and mechanisms influencing the simulated ACW-like variability differ among the different modeling studies. However, they do have some similar discrepancies when compared to the observed ACW variations.

The term "Antarctic Dipole" has been used by Yuan and Martinson (2001) to describe the leading mode of interannual variability in the southern ocean sea ice cover and surface air temperature. This variability exhibits an out-of-phase relationship between anomalies in the central/eastern Pacific and anomalies in the Atlantic sectors of the southern ocean. Dipole anomalies of this type were also discussed by Yuan and Martinson (2000) in a study on the links between Antarctic sea ice and global climate variables. This variability consists of a strong standing wave component and a weaker propagating signal within each basin. The

Antarctic Dipole has a number of similarities to the ACW, including anomalies of opposite sign in the central/eastern Pacific and Atlantic sectors and a similar period. The two are likely related. Yuan and Martinson (2001) discuss that the magnitude of the dipole variability is considerably larger than that of the ACW. They suggest that the standing wave exhibited by the Antarctic Dipole is excited by remote teleconnections and the anomalies are then advected by the ACC and/or coupled air-sea-ice interactions, contributing to the ACW variability.

Both the ACW and the Antarctic Dipole have been related to variability in the tropical Pacific, particularly the El Nino-Southern Oscillation (ENSO) (Peterson and White, 1998; Cai and Baines, 2001; Yuan and Martinson, 2000). More generally, relationships between a number of conditions at high southern latitudes and ENSO have been identified. This includes correlations with Antarctic sea ice cover (e.g. Carleton, 1988; Simmonds and Jacka, 1995; Ledley and Huang, 1997; Kwok and Comiso, 2002), oceanic conditions (e.g. Trathan and Murphy, 2003), and atmospheric properties (e.g. Karoly, 1989, Trenberth and Caron, 2000; Kidson and Renwick, 2002). These studies suggest that ENSO variability drives changes in the southern ocean. Modeling studies also suggest that other large-scale modes of variability, such as the Southern Annular Mode (SAM - also called the Antarctic Oscillation) (e.g. Thompson and Wallace, 2000) are important for forcing changes in the Antarctic ice and ocean system (Hall and Visbeck, 2002). Recent observational studies (Liu et al., 2004) also show changes in the Antarctic sea ice cover associated with the SAM.

Variability in ice and ocean conditions at high southern latitudes may also influence large-scale climate. Modeling studies have shown that changes in Antarctic sea ice modify

atmospheric (e.g. Raphael, 2003) and oceanic (Gent et al., 2001; Goosse and Fichefet, 1999; Stossel et al, 1998) conditions. Additionally, studies suggest that changes in deep and intermediate water formation in the southern ocean can modify the strength of the global thermohaline circulation and have far-reaching effects (e.g. Saenko et al., 2003).

Here we seek to understand the mechanisms driving simulated variability in ice and ocean surface conditions at high southern latitudes. Previous modeling studies have focused on simulated ACW-like behavior. In contrast, while we briefly discuss the advection of anomalies with the ACC, we focus on the standing wave pattern associated with simulated "Antarctic Dipole" variability. In particular, we address the atmosphere/ice/ocean conditions associated with the leading modes of variability in the sea ice concentration and sea surface temperature. These leading modes exhibit an Antarctic Dipole-like pattern consistent with the observations. We examine the extent to which feedbacks associated with changing ice and ocean conditions act to prolong anomalies within the southern ocean and the differences between these feedbacks in the Pacific and Atlantic sectors. The contribution of large-scale modes of variability, including ENSO and the SAM, to the Antarctic ice and ocean conditions is also explored.

For our analysis, results from a coupled climate model simulation of the Community Climate System Model version 2 (CCSM2) are used. While this, as all, model simulation has biases in its climate, it does provide a long timeseries of self-consistent data in this observationally data-sparse region. The model used for this study is discussed in section 2. The simulated ice and ocean variability is discussed in section 3. The relationship to large-scale modes of

variability, including ENSO and the SAM, is addressed in section 4. A discussion and conclusions are given in section 5.

2. Model Description

For this study, results from a control integration of the Community Climate System Model, version 2 (CCSM2) (Kiehl and Gent, 2004) are examined. This integration is run under present day conditions with no changes in anthropogenic forcing. 600 years of model integration are analyzed (Years 350-950). This time period was chosen because many of the initial climate drifts in the ice and ocean are considerably reduced by year 350 and a small change was made at year 350 in the integration allowing for consistent constants across different component models. This change had a negligible effect on the simulated climate.

CCSM2 is a state-of-the-art coupled general circulation model (GCM) that includes atmosphere, ocean, land, and sea ice components. The model has changed significantly from its initial version (Boville and Gent, 1998), with the sea ice and land components being completely modified. This has led to considerable improvements in the polar regions.

The community land model (Bonan et al., 2002) is the land surface component used within the CCSM2. The model includes a sub-grid mosaic of land cover types and plant functional types derived from satellite observations, a 10-layer soil model that explicitly treats liquid water and ice, a multi-layer snow pack model and a river routing scheme.

The ocean component of the CCSM2 uses the parallel ocean program (POP) with a number of improvements (Smith and Gent, 2002). In particular, the model uses anisotropic horizontal viscosity, an eddy mixing parameterization (Gent and McWilliams, 1990), the K-profile parameterization for vertical mixing (Large et al., 1994), and a more accurate equation of state. The horizontal resolution averages less than one degree.

The community sea ice model incorporated into CCSM2 is a new dynamic-thermodynamic scheme that includes a subgridscale ice thickness distribution (Bitz et al., 2001; Lipscomb, 2001). The model uses the energy conserving thermodynamics of Bitz and Lipscomb (1999) which has multiple vertical layers and accounts for the thermodynamic influences of brine pockets within the ice cover. The ice dynamics uses the elastic-viscous-plastic rheology of Hunke and Dukowicz (1997) with a number of updates (Hunke, 2001; Hunke and Dukowicz, 2002). Five ice thickness categories are included within each gridcell and subgridscale ridging and rafting of sea ice is parameterized following Rothrock (1975) and Thorndike et al. (1975). A discussion of the polar climate produced in this model is given by Briegleb et al. (2004).

The atmospheric component of the CCSM2 is the community atmosphere model (CAM2). It builds on the NCAR atmospheric general circulation model, CCM3 (Kiehl et al., 1996) with a number of improvements and updates. The model has enhanced resolution in the vertical, going from 18 to 26 levels. Other physics improvements include incorporation of a prognostic formulation for cloud water, a generalized geometrical cloud overlap scheme, more accurate treatment of longwave absorption/emission by water vapor, and enhancements

to the parameterization of deep cumulus convection. The model is generally run at T42 (~2.875^{o}) resolution.

3. Simulated Southern Ocean variability

3.1 Ice and ocean surface variability

The leading mode of variability obtained from an empirical orthogonal function (EOF) analysis for winter (JJAS) averaged Antarctic ice concentration exhibits a dipole pattern with anomalies of one sign in the Pacific and opposite sign in the Atlantic (Figure 1a). This mode accounts for 24% of the variance in winter ice concentration and is distinct from other modes of variability according to the separation criteria of North et al. (1982). The pattern of variability bears a strong resemblance to the "Antarctic Dipole" in observed sea ice cover discussed by Yuan and Martinson (2001), suggesting that the model is simulating realistic variability. The second and third EOFs (not shown) in simulated winter ice concentration, representing 17% and 9% of the variance, show some relationship to the leading sea ice mode, with significant correlations at minus and plus one year lag. This is associated with the limited eastward propagation of the ice concentration anomalies as discussed below.

The first EOF of annual averaged sea surface temperature (SST) in the southern ocean (south of 30S) (Figure 1b), representing 29% of the SST variance, exhibits a similar pattern to the leading sea ice mode. However, the ocean anomalies are more extensive, with considerable variations equatorward of ice formation regions. The principal component timeseries of the

leading modes of ice and SST variability are well correlated at r=0.6, with positive (negative) ice anomalies associated with cold (warm) SST. The ice variability and ocean SST variability both exhibit a red noise spectrum with dominant power at low frequencies (not shown). For this study, we are interested in the coupled ice/ocean variations in the southern ocean. As the dominant modes of variability obtained from EOF analyses represent a significant portion of the total variance and compare well to observed patterns, the following discussion will focus on these dipole-like anomalies in the Pacific and Atlantic sectors.

There is some indication that the anomalies associated with the leading modes of sea ice and SST variability propagate eastward. For example, Figure 2 shows the correlation of ice area with the principal component timeseries of the leading mode of ice variability. In general, the simulated eastward propagation is confined to the Pacific sector and does not occur consistently over the integration length. The reoccurrence of winter ice anomalies in the Pacific over a number of years and the general absence of their reoccurance in the Atlantic is related to coupled ice/ocean feedbacks as will be discussed below. The propagation speed of the simulated anomalies is slower than the observed Antarctic Circumpolar Wave speed, averaging about 4 cm/s within the Pacific basin. This is consistent with the climatological ocean currents in this region, suggesting that the anomalous surface conditions are being advected with the mean ocean circulation.

These results are similar to previous modeling studies which show ACW-like behavior (e.g. Christoph et al, 1998; Cai et al., 1999; Haarsma et al., 2000). However, in CCSM3 the anomalies do not clearly propagate around the entire Antarctic continent. Instead, they are

strongly dissipated in the eastern Atlantic and Indian Ocean. This is similar to the modeling study of Christoph et al (1998). While the observed ACW also shows the strongest signal in the Pacific region, the anomalies from approximately 1985-1995 do appear to fully encircle the globe (White and Peterson, 1996; Connolley, 2003). There are indications however, that the ACW is not continuosly present over a longer observed record (Connolley, 2003). In general, the simulated variability agrees more closely with the observed "Antarctic Dipole" variability discussed by Yuan and Martinson (2001). While recognizing that the propagation of anomalies is an important component of the simulated variability, here we focus on the Antarctic Dipole-like standing-wave anomalies in ice and SST.

The ice anomalies associated with the leading mode of ice variability are in a region of seasonal ice cover where ice area increases in the fall and winter and then completely melts away in the following spring and summer. The anomalies result from both dynamic and thermodynamic processes occurring during the ice formation seasons. Figure 3 shows the April-September average ice area tendency due to these processes for a Pacific and Atlantic region (defined in the figure caption) regressed on the leading sea ice EOF. The thermodynamic processes include all growth and melt terms and the dynamic processes include ice advection and ridging. In the Pacific basin (Figure 3a), enhanced growth rates are primarily responsible for the formation of the ice anomaly. Increased ice convergence in the fall contributes to the anomalies. However, in the winter, ice dynamics damps the anomaly by transporting more ice equatorward, out of the anomaly region, where it subsequently melts. At zero lag, this causes the April-September ice dynamic contribution to the anomalies to be near zero. The ice area tendency terms continue to be large in years lagging the ice variability,

although the dynamic and thermodynamic contributions are of opposite sign. This leads to a reduced, but still sizable, total ice area tendency associated with the ice variability. This prolongs the Pacific ice anomalies and contributes to enhanced climate memory in this region.

The Atlantic ice anomalies are also driven by a combination of dynamic and thermodynamic processes (Figure 3b). However, in contrast to the Pacific, there is little indication of anomalous conditions lagging the ice variability. This suggests that the Atlantic has less memory than the Pacific and indeed, the sea ice anomalies are shorter-lived in the Atlantic basin. This is consistent with different ocean conditions between the two basins as shown below.

Given the ocean conditions shown in Figure 1b, it is not surprising that thermodynamics contribute to the formation of the ice anomalies. An analysis of the ice/ocean heat flux and basal ice growth associated with the sea ice EOF (not shown) is consistent with the ocean surface conditions contributing to the ice concentration anomalies. The temperature anomalies associated with the first EOF of SST are not confined to the surface, particularly in the Pacific, where they extend down to hundreds of meters in depth. The temperature anomalies result from changes in ocean circulation and/or changes in the ocean surface heat flux. In the Pacific basin, changes in ocean circulation dominate. Figure 4 shows the ocean heat flux convergence regressed on the dominant mode of SST variability. The ocean heat flux convergence represents the total depth integrated value and is computed as a residual:

$$\int_0^D \nabla \cdot F_{horiz} dz = F_{net} - \int_0^D c_w \frac{\partial T_w}{\partial t} dz$$

where, the first term represents the depth integrated horizontal ocean heat flux convergnce,

F_{net} is the net surface heat flux into the ocean, and the last term represents the changes in the depth integrated ocean heat content, with c_w equal to the ocean heat capacity and T_w equal to the ocean temperature. The depth integrated ocean heat flux convergence shows considerable changes in the Pacific associated with the SST variability, with large regions of the regression exceeding 10 W m^{-2}. The decreased ocean heat flux convergence over much of the Pacific sector of the southern ocean is consistent with an increased meridional velocity transporting more cold water away from the Antarctic continent. The increased meridional transport extends to several thousand meters in depth. Additionally, there is increased upwelling in the high southern latitudes of the Pacific which enhances the cold SST anomalies.

In the Atlantic, the ocean temperature changes associated with the first EOF of SST are confined to the upper hundred meters. Changes in the column integrated ocean heat flux convergence (Figure 4) within the Atlantic sector are smaller and less coherent than those in the Pacific. No single mechanism dominates in driving the Atlantic SST anomalies. Instead, there are modest contributions from a number of processes, including changes in the surface ocean circulation and surface heat fluxes. Both turbulent heat exchange and absorbed solar radiation anomalies contribute to the high Atlantic surface heat fluxes associated with the SST variability. While the high solar absorption is likely associated with the low ice cover, the change in sensible heating occurs in spite of it. In particular, the anomalously low Atlantic sea ice causes a reduced insulating effect which allows the ocean to lose more heat to the atmosphere. This is not the case because of the anomalously warm atmospheric conditions associated with the SST variability as discussed in section 3.2.

The SST variability influences the thermodynamic forcing of the ice anomalies. Additionally, there are feedbacks associated with the anomalous ice cover which act to modify the surface ocean conditions following the ice anomalies and help to prolong the life of the anomalies. In particular, the increased Pacific ice cover reduces the length of the summer ice-free season and the solar radiation absorbed by the ocean the following spring (Figure 5). This results in colder SSTs, and increased ice growth rates in the following year. This allows ice anomalies to reform in subsequent winters in the Pacific region and leads to the longer memory in this region. The anomalies propagate eastward because the SST conditions and their influence on sea ice are transported with the ocean currents. This is similar to the mechanism proposed by Gloersen and White (2001) to explain the reoccurrence of sea ice anomalies associated with the ACW.

In the Atlantic, as discussed above, more solar radiation is absorbed (Figure 5) and warmer SSTs are present in the region of anomalous ice conditions. However, this does not substantially reinforce the sea ice anomalies in the western Atlantic in following years. This is related to the influence of the climatological ocean currents (Figure 6) on the anomalous ocean conditions. The ocean currents are relatively strong in the region of the SST anomalies and have a considerable northward component. This transports the anomalously warm ocean waters to a region where no sea ice formation occurs and thus they no longer result in ice anomalies. This short-circuits the sea ice-albedo feedback and reduces the lifetime of anomalous conditions within the Atlantic.

3.2 Atmospheric conditions associated with southern ocean surface variability

As shown above, both dynamic and thermodynamic processes are important for driving the ice and surface ocean anomalies associated with the leading modes of variability. Presumably these processes are related to the atmospheric state. Additionally, feedbacks associated with the ice and ocean conditions can modify the atmosphere.

Figure 7 shows the linear regression of annual average sea level pressure (SLP) on the leading modes of sea ice and ocean SST variability. These show a similar structure with below normal SLP over the Antarctic continent and the ocean south of approximately 55S surrounded by a band of higher than normal SLP to the north. An anomalous low pressure center is located over the Amundsen/Bellingshausen Sea in both analysis, although it is more localized in the sea ice analysis.

The geostrophic winds associated with the simulated SLP pattern generally result in anomalous westerly flow around the Antarctic continent, which drives enhanced Ekman equatorward ocean transport. Additionally, the anomalous low pressure centered in the Amundsen-Bellingshausen sea results in enhanced equatorward ice and ocean transport in the Pacific sector, but reduced equatorward transport in the Weddell Sea region. This is consistent with the ice drift and ocean heat flux convergence anomalies associated with the leading modes of ice and SST variability. Anomalies in SLP are most highly correlated to the ice and SST variability at zero-lag. Significant correlations are also found with the SLP leading the ice variations by 10 months, suggesting that the atmosphere is in part forcing the ice

variations. There is little indication that the SST or ice anomalies are in turn driving SLP variations and the SLP anomalies are minimal following the anomalous ice and ocean conditions.

Surface air temperature changes are also associated with the leading modes of sea ice and SST variability (Figure 8). These anomalies are similar for both the ice and SST regressions and are consistent with anomalous atmospheric heat transport associated with the SLP patterns discussed above. These SAT anomalies would contribute to the thermodynamic forcing of the ice and SST modes of variability. Correlations between the SAT and the ice and ocean variability are highest at zero-lag, but are significant over an extended period of time. In particular, Pacific SAT from the preceding summer shows enhanced (negative) correlations with the sea ice variability, reaching absolute values greater than r=0.5. This is likely related to the relatively long timescales of the ice anomalies within the Pacific.

There are also indications that the SAT anomalies continue into the years following the ice and ocean variations. This is particularly true in the Pacific where low SATs are present and correlations between the SAT and ice and ocean conditions remain significant for 1-2 years following the ice and ocean variations. Due to the anomalously large ice cover in the Pacific, there is reduced turbulent heat exchange into the atmosphere. This acts to reinforce the SAT anomalies. Additionally, as discussed above ocean-ice feedbacks, associated with changes in absorbed solar radiation affect the SST anomalies and extend the life of the sea ice anomalies, allowing them to reform in the Pacific in following years. In the Atlantic, the SAT anomalies associated with the ice and ocean variability are not as large or as long-lived as those in the

Pacific. As discussed above, this difference between the Pacific and Atlantic basins is related to the mean ocean circulation. In the Pacific, the SST anomalies are transported eastward by the mean ocean circulation and affect ice growth rates in the following fall. In the Atlantic, the ocean circulation transports the anomalies away from the ice formation region, reducing their impact on the atmospheric conditions.

4. Relationship to large scale modes of variability

A number of observational studies (e.g. Simmonds and Jacka, 1995: Ledley and Huang, 1997; Peterson and White, 1998; Yuan and Martinson, 2000; Cai and Baines, 2001; Kwok and Comiso, 2002) have suggested that there is a relationship between the El Nino - Southern Oscillation (ENSO) and southern ocean conditions. Peterson and White (1998) and Cai and Baines (2001) have linked forcing of the Antarctic Circumpolar Wave to ENSO teleconnections. Kwok and Comiso (2002) have shown that, associated with ENSO events, there is reduced ice cover in the Ross and Amundsen Seas and increased ice cover in the Bellingshausen and Weddell Seas. This has a similar spatial structure (with opposite sign) to that seen in the first EOF of winter sea ice area shown in Figure 1a and suggests that there may be some relationship between the two. Yuan and Martinson (2000) also found that the observed "Antarctic Dipole" was significantly correlated to ENSO events.

Additionally, recent studies have examined the influence of the southern annular mode (SAM) on ice and ocean conditions in both model simulations (Hall and Visbeck, 2002) and in observations (Liu et al, 2004). Both these studies show significant relationships to the

Antarctic sea ice variability, although the spatial distribution of the relationship differs.

Here we examine the influence of the simulated ENSO and SAM on the southern ocean variability. This includes an analysis of how ENSO and SAM relate to the leading modes of sea ice and SST variability discussed above.

4.1 ENSO Variability

The ENSO variability in the CCSM2 simulation is somewhat weaker than observed and has a shorter dominant timescale of roughly 2-3 years (Kiehl and Gent, 2004). Here we use the NINO3 SST timeseries as a measure of ENSO variability.

In general, the teleconnections between ENSO and the southern ocean appear reasonable. Figure 9a shows the monthly SLP anomalies regressed on the monthly NINO3 timeseries. The spatial pattern exhibits a Pacific-South American pattern similar to the observations (Karoly, 1989) and compares well with other recent observational analysis (e.g. Trenberth and Caron, 2000; Cai and Baines, 2001; Kidson and Renwick, 2002; Kwok and Comiso, 2002). As will be shown below, the leading mode of Antarctic sea ice variability is most strongly correlated to the NINO3 index from the previous January. In a regression of SLP from other months onto the January NINO3 SST, we find that enhanced regressions are obtained with the July SLP (Figure 9b). The maximum linear regression is similar to the January values at zero lag, but the center of the anomalous high is shifted eastward to a region where it has a more direct influence on meridional ice transport in the Atlantic and Pacific regions. These July

SLP anomalies are similar in location (but opposite in sign) to those associated with the leading modes of the simulated surface ocean variability (Figure 7), particularly the sea ice conditions.

There are also winter SAT anomalies near the Antarctic continent associated with the NINO3 SST from the previous January (not shown), that closely resemble (with opposite sign) those associated with the leading mode of ice variability (Figure 8). It is likely that these are partially driven by SLP related changes in atmospheric heat transport. It is also likely that the SAT is responding to wind driven changes in the sea ice and SST.

The SAT and SLP variability associated with ENSO thermodynamically and dynamically force sea ice and ocean surface conditions that have a dipole like structure. A map of sea ice and SST regressed on the January NINO3 timeseries (Figure 10), confirms this relationship. This variability has a similar spatial pattern as the first EOF of sea ice (Figure 1a) and the first EOF of SST (Figure 1b). Figure 11 shows the correlation between the monthly NINO3 timeseries and the principle components of these two different EOFs. As mentioned above, the maximum correlations are obtained when NINO3 leads the ice conditions by approximately six months, indicating that the winter ice variability is responding to ENSO events in the preceding austral summer.

The relatively weak correlation and small ice and SST anomalies associated with ENSO indicates that over the whole integration, ENSO is influencing the southern ocean conditions but is not the dominant factor in the variability. It is possible that the timescales associated

with the simulated ENSO reduce its influence on the southern ocean variability compared to the real world. In particular, the dominance of a two year timescale means that an El Nino event is quickly followed by a La Nina event. This may not allow the ice and ocean anomalies to build over a number of years and may reduce the total surface variability associated with ENSO in this region.

4.2 Southern Annular Mode Variability

The dominant mode of southern hemisphere sea level pressure (SLP) variability in both the observations and CCSM2 simulations is characterized by fluctuations in the strength of the circumpolar vortex (Figure 12) (e.g. Thompson and Wallace, 2000). Observations (Liu et al, 2004) suggest that a relationship exists between this mode of variability and the southern hemisphere ice cover. This supports GCM model results which show ice and southern ocean anomalies associated with the simulated SAM (Hall and Visbeck, 2002). Hall and Visbeck find that the enhanced westerlies at approximately 55S associated with a positive SAM index, drive equatorward Ekman flow in the ocean at high latitudes. This results in anomalous northward transport of sea ice, leading to increased ice cover, particularly in the Indian Ocean sector. These model simulations provide reasonable physical mechanisms related to the influence of SAM on the ocean and ice conditions. However, the maximum simulated variations in ice cover occur in a region where the observations indicate low variability and the spatial pattern of the simulated ice anomalies is different than those seen in the observations (Liu et al., 2004). Here we examine the influence of SAM on the simulated ice and surface ocean variability in the CCSM2.

The simulated SAM exhibits anomalous low SLP at high latitudes surrounded by a band of higher SLP. This is very similar to the SLP regressed on the leading mode of SST variability (Figure 7b). This SLP pattern results in enhanced westerly winds at approximately 60S in the model. The climatological surface temperatures generally exhibit warmer conditions over the oceans at these latitudes. This coupled with the enhanced westerly winds associated with SAM, result in changes in the air temperature advection which cause a warming near the Antarctic peninsula and a small cooling near the Ross Sea (Figure 13a). Additionally there is cooling over much of the Antarctic continent. These features are consistent with recent trends in the Antarctic climate that have been linked to the observed SAM (Thompson and Solomon, 2002).

As found by Hall and Visbeck (2002), changes in the simulated ocean circulation are associated with the simulated SAM. A regression of the surface currents on the SAM index reveals enhanced equatorward flow at high latitudes (Figure 13b). This drives anomalous ice transport northward and also modifies the ocean heat transport. In most of the Pacific basin and Indian Ocean south of 55S, this generally leads to a decrease in advective ocean heat flux convergence at the surface as more cold water is transported northward. Enhanced upwelling also contributes to the SST anomalies. In the Atlantic and western Pacific, only small changes in advective heat flux convergence are present. This is probably related to smaller anomalous meridional ocean transport in these regions as shown in Figure 13b and in the Atlantic to a reduced meridional SST gradient.

The SST anomalies associated with SAM are shown in Figure 13c. They exhibit a dipole-like pattern and the forcing mechanisms are very similar to those associated with the first EOF of SST. In particular, changes in ocean heat flux convergence are important in the Pacific. Whereas, in the Atlantic, the net surface heat fluxes associated with the SAM act to warm the surface ocean, due to decreased ocean turbulent heat loss and enhanced solar absorption. The SAM index and SST EOF principal component are significantly correlated at r=0.6, suggesting that the dominant mode of SST variability results in part from a response to the atmospheric forcing associated with the SAM.

The SAT and SST anomalies associated with the SAM influence thermodynamic ice growth rates. Additionally, the SAM induced wind anomalies modify the ice transport. The resulting ice anomalies associated with the SAM are largest lagging the SAM index by one year. They exhibit a pattern with reduced ice in the western Atlantic and increased ice across much of the Pacific and Indian Ocean regions (Figure 13d). The anomalies of opposite sign between the Atlantic and Pacific regions resembles the first EOF of sea ice variability although the ice anomalies associated with SAM are considerably smaller.

In both the Pacific and Indian sectors, dynamic and thermodynamic processes enhance the ice area coincident with SAM. The anomalous ice growth is related to the cold SAT and the anomalously low ocean heat flux convergence in these regions. A year later, the anomalous ice growth is considerably higher leading to more sizable anomalies lagging the SAM index by one year. This lagged relationship is related to the ice-albedo feedback enhancing the initial ice anomaly due to lower oceanic shortwave absorption and colder SST conditions.

In the Atlantic, reduced ice cover is associated with the SAM. Although the ocean currents are anomalously northward, there is reduced equatorward ice transport in autumn due to low ice growth rates which reduce the amount of ice towards the continent that can be transported. Low ice growth rates also directly reduce the Atlantic ice cover in winter. The differences in ice conditions associated with the SAM in the Atlantic and Pacific/Indian sectors of the southern ocean are related to different atmospheric conditions in the two regions and the relative roles of the ocean and atmosphere in forcing the ice variability. In the Atlantic, changes in ocean circulation and heat flux convergence are less important due in part to different mean ocean conditions.

Overall, the SAM and leading mode of sea ice variability are weakly correlated at r=0.35 with the ice lagging the SAM by one year. SAM and ENSO have a comparable influence on the Antarctic sea ice variations, with both contributing weakly to the ice variability. The SAM also contributes to sea ice variability in the Indian sector and is more highly correlated to the variations in SST. From the coherency spectrum (Figure 14), we can examine the correlation of SAM and ENSO with the leading modes of southern ocean variability as a function of frequency. This indicates that the SAM is more important for the low frequency fluctuations in the sea ice. The variability associated with ENSO has less dependence on frequency.

5. Summary and Conclusions

Variations in the surface southern ocean conditions, specifically the sea ice cover and sea surface temperatures (SST), in a climate integration of the CCSM2 have been examined. The leading modes of variability in sea ice concentration and SST exhibit anomalies of one sign in the Atlantic sector associated with anomalies of the opposite sign in the Pacific. The SST anomalies, while largest in the Pacific sector, are more extensive than the ice anomalies with considerable variations in SST equatorward of the ice formation regions. These anomalous simulated conditions are consistent with observations of the "Antarctic Dipole" which has positive sea ice anomalies in the Pacific associated with negative anomalies in the Atlantic (e.g. Yuan and Martinson, 2001).

This "Antarctic Dipole" pattern of sea ice variability is forced by a combination of both thermodynamic and dynamic processes that are consistent with the atmospheric conditions. In particular, anomalously low SLP in the Amundsen/Bellingshausen Sea leads and is coincident with the changes in sea ice. This suggests that the atmosphere is in part forcing the sea ice variations. The ocean conditions, particularly Pacific SST variations, are also instrumental in forcing the ice anomalies. These SST changes are largely driven by changes in ocean circulation that are consistent with the atmospheric circulation anomalies. In the Atlantic, no single mechanism dominates in forcing the ice and SST anomalies. Instead, changes in surface heat fluxes and surface circulation both contribute.

Ice/ocean coupling, in particular feedbacks associated with the surface albedo and insulating

effect of the sea ice, contribute to an enhanced memory in the southern ocean. These feedbacks are present even though the ice anomalies occur in a region of seasonal ice cover. Changes in the ocean shortwave absorption are forced by the anomalous sea ice conditions. This reinforces the anomalous ocean SSTs and allows the ice anomalies to reform in subsequent years. This is particularly true in the Pacific sector, where the anomalies are transported eastward with the Antarctic Circumpolar Current but remain relatively close to the continent within the ice formation region. The anomalous surface conditions feedback to the surface air temperature which helps reinforce the ice and SST anomalies over multiple years. However, from the correlation analysis done here, the sea level pressure appears to have little response.

In the Atlantic sector, the ice anomalies are shorter lived and have little eastward propagation. These Atlantic ice anomalies form in a region where there is a considerable northward component to the surface ocean velocity. Although the ice anomalies result in changes in the absorbed solar radiation, these anomalous conditions are transported to a region where they no longer affect ice formation. This short-circuits the ice albedo feedback mechanism, resulting in shorter-lived anomalies which exhibit little eastward propagation.

Large scale modes of variability, such as ENSO and the Southern Annular Mode (SAM), contribute to the simulated sea ice and SST variability in the southern ocean. Interestingly, both ENSO and SAM drive "Antarctic Dipole" type anomalies, with anomalies of one sign in the Atlantic and of opposite sign in the Pacific. They both weakly contribute to the leading mode of sea ice variability, whereas the SAM is more important in forcing the SST variations.

Acknowledgements: The authors would like to thank Dr. Peter Gent for comments on a draft manuscript of this work and Dr. Marilyn Raphael for useful discussions during the course of this study. Thanks is also given to the numerous researchers involved in the development of the CCSM2. We also appreciate the constructive comments given by two anonymous reviewers. ECH was supported under the U.S. Department of Energy's Climate Change Prediction Program. NCAR is supported by the National Science Foundation.

References

Bitz, C.M., M.M. Holland, M. Eby, and A.J. Weaver, 2001: Simulating the ice-thickness distribution in a coupled climate model, *J. Geophys. Res*., **106**, 2441-2463.

Bitz, C. M. and W. H. Lipscomb, 1999: An energy-conserving thermodynamic model of sea ice. *J. Geophys. Res*., **104**, 15669-15677.

Bonan, G. B., K. W. Oleson, M. Vertenstein, S. Levis, X. Zeng, Y. Dai, R.E. Dickson, and Z-L Yang, 2002: The land surface climatology of the Community Land Model coupled to the NCAR Community Climate Model. *J. Climate* (submitted).

Boville, B.A. and P.R. Gent, 1998: The NCAR Climate System Model, version one. *J. Climate,* **11**, 1115-1130.

Briegleb, B. P., *et al., 2004: The sea ice simulation of the Community Climate System Model, version two. NCAR Technical Note, NCAR/TN-45+STR, 34 pp.

Cai, W., P.G. Baines, and H.B. Gordon, 1999: Southern mid- to high-latitude variability, a zonal wavenumber-3 pattern, and the Antarctic circumpolar wave in the CSIRO coupled model. *J. Climate*, **12**, 3087-3104.

Cai, W., and P.G. Baines, 2001: Forcing of the Antarctic Circumpolar Wave by El Nino-Southern Oscillation teleconnections, *J. Geophys. Res.*, **106**, 9019-9038.

Carleton, A.M., 1988: Sea ice atmosphere signal of the Southern Oscillation in the Weddell Sea, Antarctica. *J. Climate*, **1**, 379-388.

Christoph, M., T.P. Barnett, and E. Roeckner, 1998: The Antarctic Circumpolar Wave in a coupled atmosphere-ocean GCM. *J. Climate*, **11**, 1659-1672.

Gent P. R. and J. C. McWilliams, 1990: Isopycnal mixing in ocean circulation models. *J. Phys. Ocean.,* **20**, 150-155.

Gent, P. R., W. G. Large, and F. O. Bryan, 2001: What sets the mean transport through Drake Passage? *J. Geophys. Res.,* **106**, 2693-2712.

Gloersen, P., and W.B. White, 2001: Reestablishing the circumpolar wave in sea ice around Antarctica from one winter to the next. *Geophys. Res. Lett.*, **106**, 4391-4395.

Goosse, H., and T. Fichefet, 1999: Importance of ice-ocean interactions for the global ocean circulation: A model study. *J. Geophys. Res.*, **104**, 23,337-23,355.

Haarsma, R.J, F.M. Selten, and J.M. Opsteegh, 2000: On the mechanism of the Antarctic Circumpolar Wave. *J. Climate,* **13**, 1461-1480.

Hall, A., and M. Visbeck, 2002: Synchronous variability in the southern hemisphere atmosphere, sea ice and ocean resulting from the annular mode. *J. Climate*, **15**, 3043-3057.

Hunke, E.C. and J. K. Dukowicz, 1997: An Elastic-viscous-plastic model for sea ice dynamics. *J. Phys. Ocean.,* **27**, 1849-1867.

Hunke, E.C., 2001: Viscous-plastic sea ice dynamics with the EVP model: Linearization issues, *J. Computational Physics*, **170** (1), 18-38.

Hunke, E.C., and J.K. Dukowicz, 2002: The elastic-viscous-plastic sea ice dynamics model in general orthogonal curvilinear coordinates on a sphere-incorporation of metric terms. *Monthly Weather Review*, **130**(7), 1848-1865.

Jacobs, G.A., and J.L. Mitchell, 1996: Ocean circulation variations associated with the Antarctic Circumpolar Wave. *Geophys. Res. Lett.*, **23**, 2947-2950.

Karoly, D.J., 1989: Southern hemisphere circulation features associated with El Nino-Southern Oscillation events, *J. Climate*, **2**, 1239-1252.

Kidson, J.W., and J.A. Renwick, 2002: The southern hemisphere evolution of ENSO during 1981-1999. *J. Climate*, **15**, 847-863.

Kiehl, J. T., and P. R. Gent, 2004: The Community Climate System Model, version two. *J. Climate*, in press.

Kiehl, J.T., J.J. Hack, G.B. Bonan, B.A. Boville, B.P. Briegleb, D.L. Williamson, P.J. Rasch, 1996: Description of the NCAR Community Climate Model (CCM3), NCAR Technical Note, NCAR/TN-420+STR, 152pp.

Kwok, R., and J.C. Comiso, 2002: Southern ocean climate and sea ice anomalies associated with the Southern Oscillation, *J. Climate*, **15**, 487-501.

Large W.G., J. C. McWilliams and S.C. Doney, 1994: Oceanic vertical mixing: A review and a model with a nonlocal boundary layer parameterization. *Rev. Geophys*., **32**, 363-403.

Ledley, T.S. And Z. Huang, 1997: A possible ENSO signal in the Ross Sea. *Geophys. Res. Lett.*, **24**, 3253-3256.

Lipscomb, W.H., 2001: Remapping the thickness distribution in sea ice models, *J. Geophys. Res.*, **106**, 13,989-14,000.

Liu, J., J.A. Curry, D.G. Martinson, 2004. Interpretation of recent Antarctic sea ice variability, *Geophys. Res. Lett.*, **31**, L02205, doi:10.1029/2003GL018732.

Peterson, R.G., and W.B. White, 1998: Slow oceanic teleconnections linking the Antarctic Circumpolar Wave with the tropical El Nino-Southern Oscillation, *J. Geophys. Res.*, **103**, 24,573-24,583.

Raphael, MN, 2003: Impact of observed sea-ice concentration on the Southern Hemisphere extratropical atmospheric circulation in summer, *J. Geophys. Res.*, **108**(D22), 4687.

Rothrock, D.A., 1975: The energetics of the plastic deformation of pack ice by ridging, *J. Geophys. Res*., **80**, 4514-4519.

Saenko, O.A., A.J. Weaver, and J.M. Gregory, 2003: On the link between the two modes of the ocean thermohaline circulation and the formation of global-scale water masses. *J. Climate*, **16**, 2797-2801.

Simmonds, I. and T.H. Jacka, 1995: Relationships between the interannual variability of Antarctic sea ice and the Southern Oscillation, *J. Climate*, **8**, 637-647.

Smith R. and P. Gent (eds), 2002: Reference manual for the Parallel Ocean Program ocean component of the Community Climate System Model (CCSM2.0), NCAR. Available at *http://www.ccsm.ucar.edu/models*.

Stossel, A., S.J. Kim, and S.S. Drijfhout, 1998: The impact of southern ocean sea ice in a global ocean model. *J. Phys. Oceanogr.*, **28**, 1999-2018.

D.W. Thompson, and S. Solomon, 2002: Interpretation of recent Southern hemisphere climate change. *Science*, **296**, 895-899.

Thompson, D.W., and J.M. Wallace, 2000: Annual modes in extratropical circulation, Part I: Month-to-Month Variability, *J. Climate*, **13**, 1000-1016.

Thorndike, A.S., D.S. Rothrock, G.A. Maykut, and R. Colony, 1975: Thickness distribution of sea ice. *J. Geophys. Res.*, **80**, 4501-4513.

Trathan, P.N., and E.J. Murphy, 2002: Sea surface temperature anomalies near South Georgia: Relationships with the pacific El Nino regions. *J. Geophys. Res.*, **108** (C4), 8075.

Trenberth, K.E., and J.M. Caron, 2000: The Southern Oscillation revisited: Sea level pressures, surface temperatures, and precipitation. *J. Climate*, **13**, 4358-4365.

White, W.B., and R.G. Peterson, 1996: An Antarctic circumpolar wave in surface pressure, wind, temperature and sea ice extent, *Nature*, **380**, 699-702.

Yuan, X. and D.G. Martinson, 2000: Antarctic sea ice extent variability and its global connectivity, *J. Climate*, **13**, 1697-1717.

Yuan, X., and C.G. Martinson, 2001: The Antarctic Dipole and its predictability, *Geophys. Res. Lett.*, **28**(18), 3609-3612.

Figures

1. The first EOF of simulated (a) winter (JJAS) ice concentration and (b) annual averaged sea surface temperature (SST) for the southern ocean south of 30S. The nondimensional EOFs have been scaled by the standard deviation of the corresponding principal component timeseries to show the dimensional standard deviation at each grid point associated with the EOF. The contour interval is 5% for sea ice and 0.1^{o}C for SST. The zero contour has been omitted and positive values are shaded. In panel a, the 10% contour interval is bold and denotes the region used in the budget analysis shown in Figure 3.

2. The correlation of the leading mode of ice concentration variability and the ice area as a function of longitude and lag. The contour interval is 0.1 and positive values are shaded. Southern hemisphere continental outlines are shown at the bottom of the plot for reference.

3. The AMJJAS averaged ice area tendency regressed on the leading mode of ice concentration variability. The total tendency (diamonds), contribution due to thermodynamic processes (+) and contribution due to dynamic processes (*) are shown. The analysis is performed for (a) the Pacific and (b) the Atlantic regions where the ice concentration anomalies associated with the sea ice EOF are greater than 10% fractional coverage. These regions are denoted on Figure 1 by the thick contour.

4. The regression of annual averaged ocean heat flux convergence on the leading mode of SST variability. The contour interval is 5 W m^{-2} and positive values are shaded.

5. The solar radiation absorbed in the ocean regressed on the leading mode of sea ice variability. The contour interval is 1 W m^{-2}, the zero contour is omitted, and positive values are shaded.

6. The climatological ocean surface velocity.

7. Annual averaged SLP regressed on the a) leading mode of sea ice variability and b) leading mode of SST variability. The contour interval is 0.5 mb per standard deviation of the principal component timeseries and positive values are shaded.

8. Annual averaged SAT regressed on the a) leading mode of sea ice variability and b) leading mode of SST variability. The contour interval is 0.2^{o}C per standard deviation of the principal component timeseries and positive values are shaded.

9. The (a) monthly SLP anomalies regressed on the monthly averaged NINO3 timeseries and (b) July SLP anomaly regressed on the previous January NINO3 timeseries. The contour interval is 0.5 mb per standard deviation of the NINO3 timeseries and positive values are shaded.

10. (a) JAS sea ice concentration and (b) annual averaged SST regressed on the January NINO3 timeseries. The contour interval is 2% fractional coverage in (a) and 0.1^{o}C in (b) per standard deviation of the NINO3 timeseries. Positive values are shaded and the zero contour

is not shown in (a).

11. Correlation of the monthly NINO3 timeseries and the principal component of the leading mode of winter sea ice variability (*) and the leading mode of annual average SST variability (diamonds).

12. The first EOF of sea level pressure for the southern hemisphere from 20 to 90S. The nondimensional EOF has been scaled by the standard deviation of the corresponding principal component timesereis to show the dimensional standard deviation of SLP at each grid point associated with the EOF. The contour interval is 0.5 mb and positive values are shaded.

13. Climate variables regressed on the normalized SAM index. Shown are a) SAT, with a contour interval of 0.2 ^{o}C, b) ocean surface velocity, c) SST, with a contour interval of 0.1 ^{o}C, and d) winter ice concentration lagged by one year, with a contour interval of 2% fractional coverage. Positive values are shaded and the zero contour interval is omitted from panel d.

14. The squared coherency spectrum of the leading mode of sea ice variability with the SAM (solid line) and with the January NINO3 timeseries (dashed line).

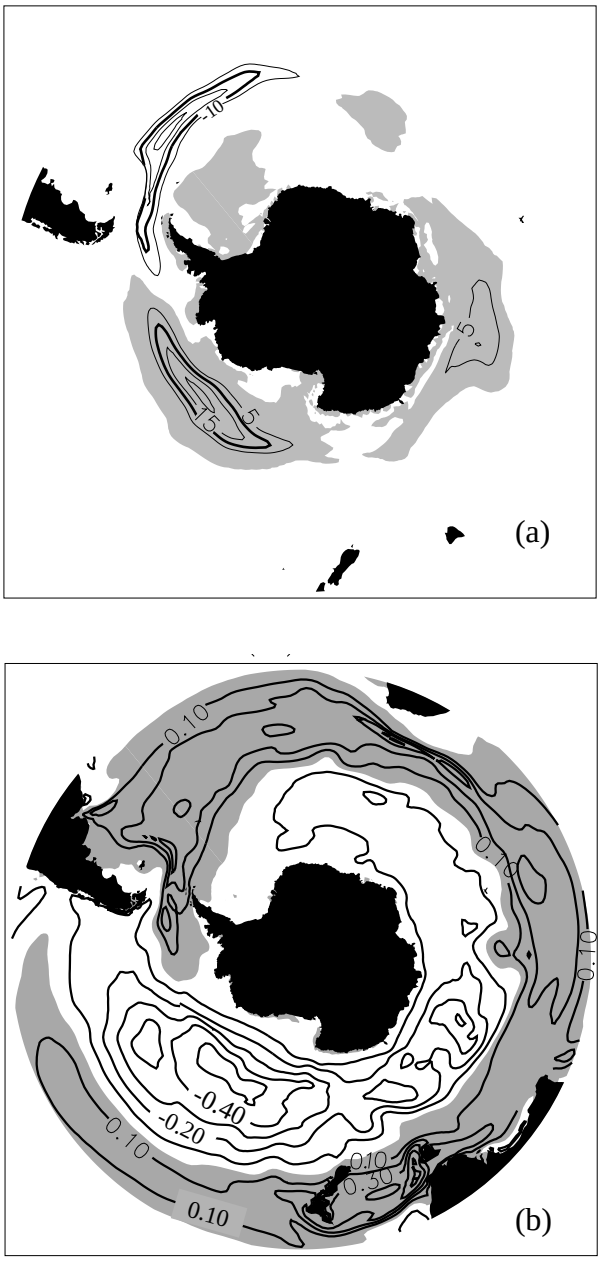

Figure 1. The first EOF of simulated (a) winter (JJAS) ice concentration and (b) annual averaged sea surface temperature (SST) for the southern ocean south of 30S. The nondimensional EOFs have been scaled by the standard deviation of the corresponding principal component timeseries to show the dimensional standard deviation at each grid point associated with the EOF. The contour interval is 5% for sea ice and 0.1^{o}C for SST. The zero contour has been omitted and positive values are shaded. In panel a, the 10% contour interval is bold and denotes the region used in the budget analysis shown in Figure 3.

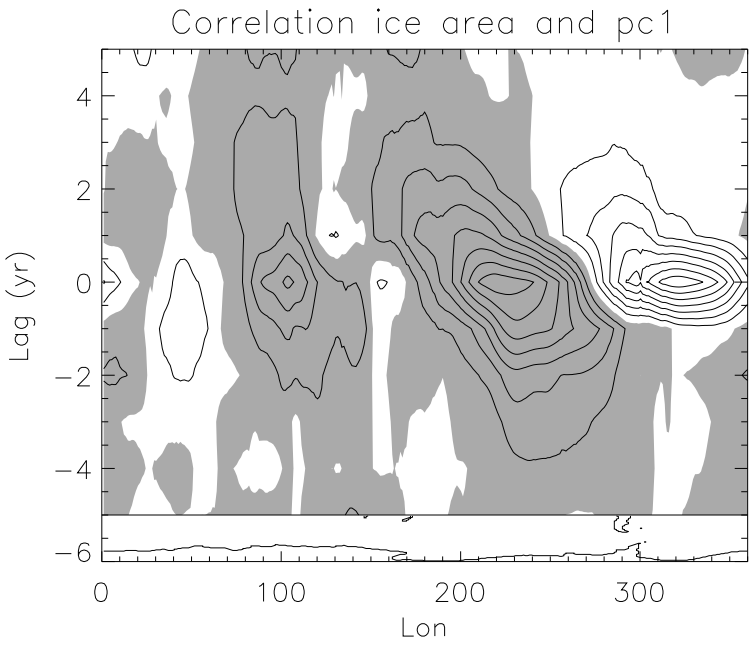

Figure 2. The correlation of the leading mode of ice concentration variability and the ice area as a function of longitude and lag. The contour interval is 0.1 and positive values are shaded. Southern hemisphere continental outlines are shown at the bottom of the plot for reference.

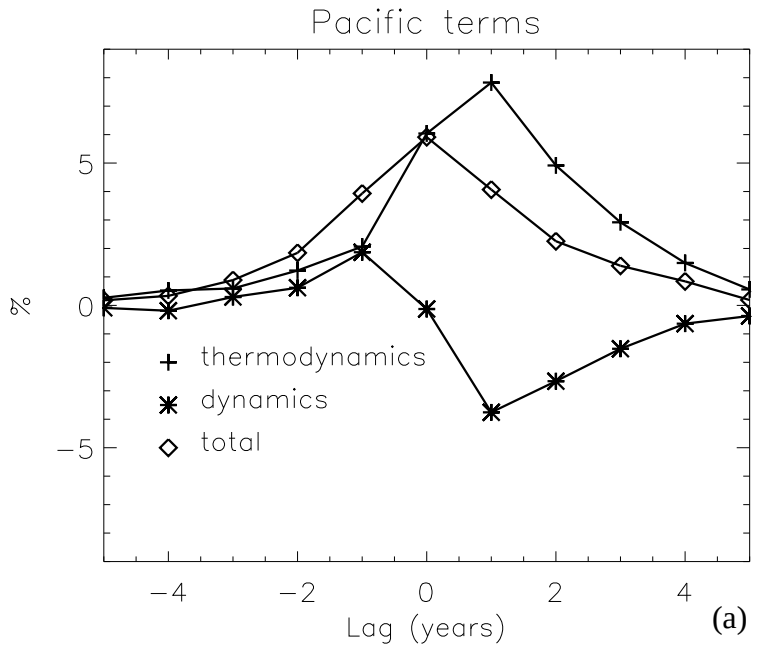

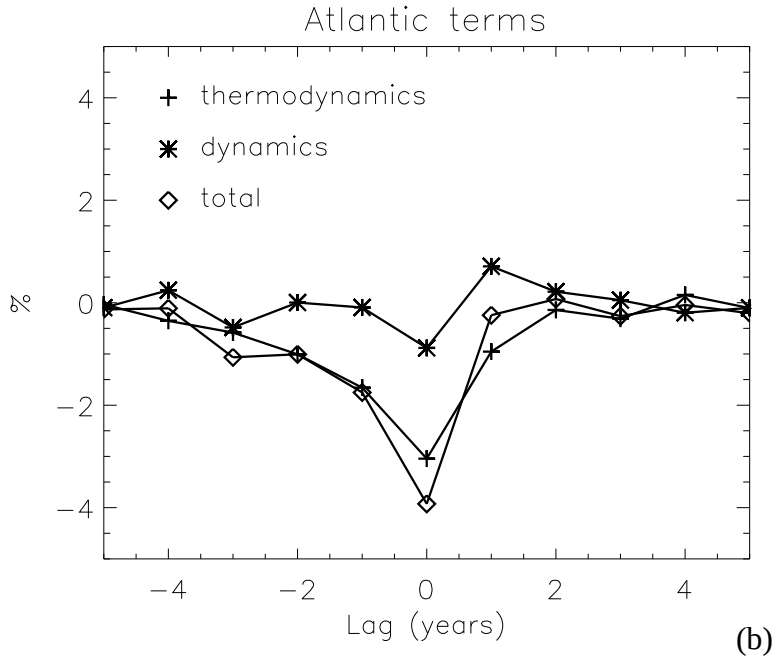

Figure 3. The AMJJAS averaged ice area tendency regressed on the leading mode of ice concentration variability. The total tendency (diamonds), contribution due to thermodynamic processes (+) and contribution due to dynamic processes (*) are shown. The analysis is performed for (a) the Pacific and (b) the Atlantic regions where the ice concentration anomalies associated with the sea ice EOF are greater than 10% fractional coverage. These regions are denoted on Figure 1 by the thick contour.

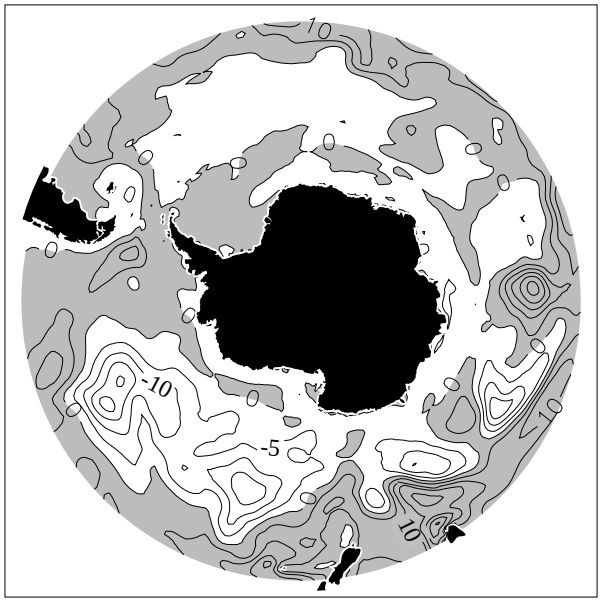

Figure 4. The regression of ocean heat flux convergence on the leading mode of SST variability. The contour interval is 5 W m^{-2} and positive values are shaded.

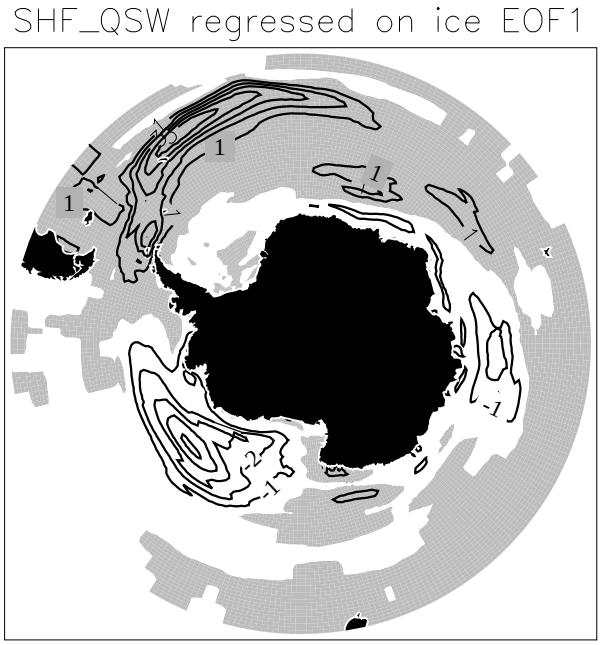

Figure 5. The solar radiation absorbed in the ocean regressed on the leading mode of sea ice variability. The contour interval is 1 W m^{-2}, the zero contour is omitted and positive values are shaded.

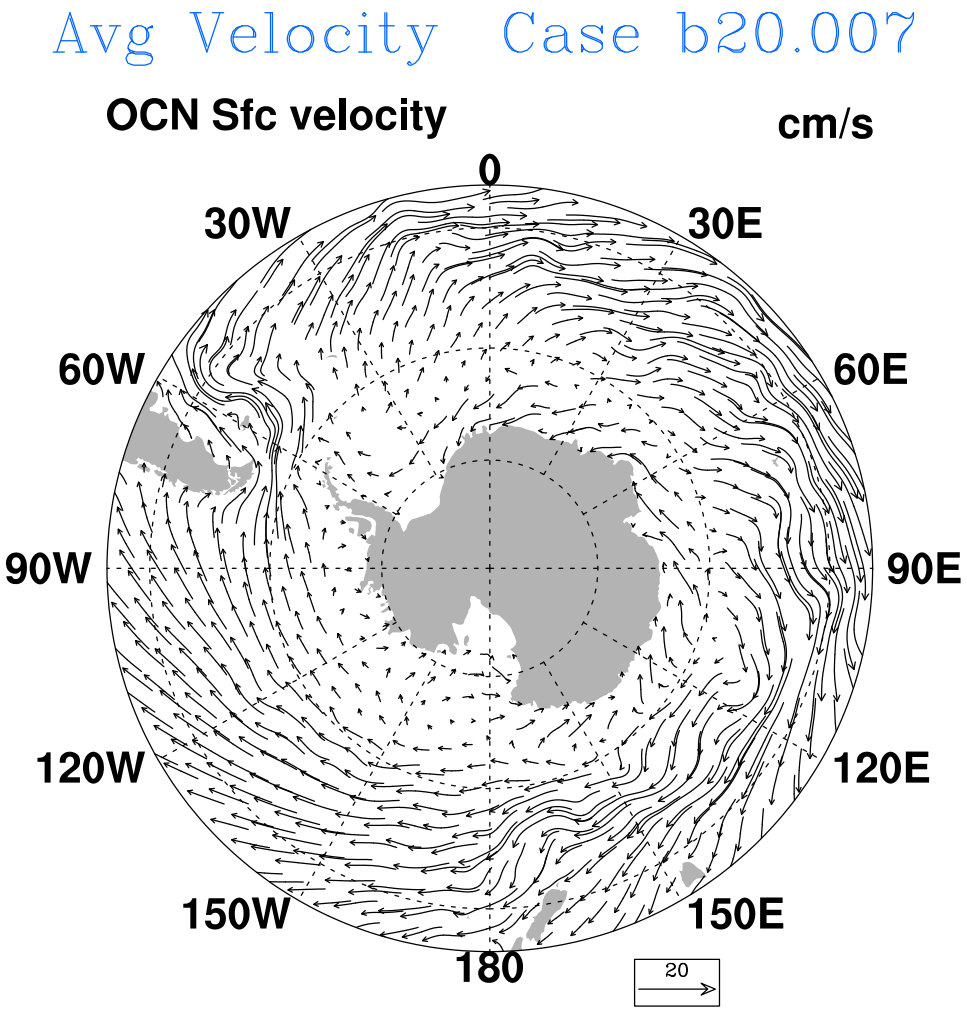

Figure 6. The climatological ocean surface velocity.

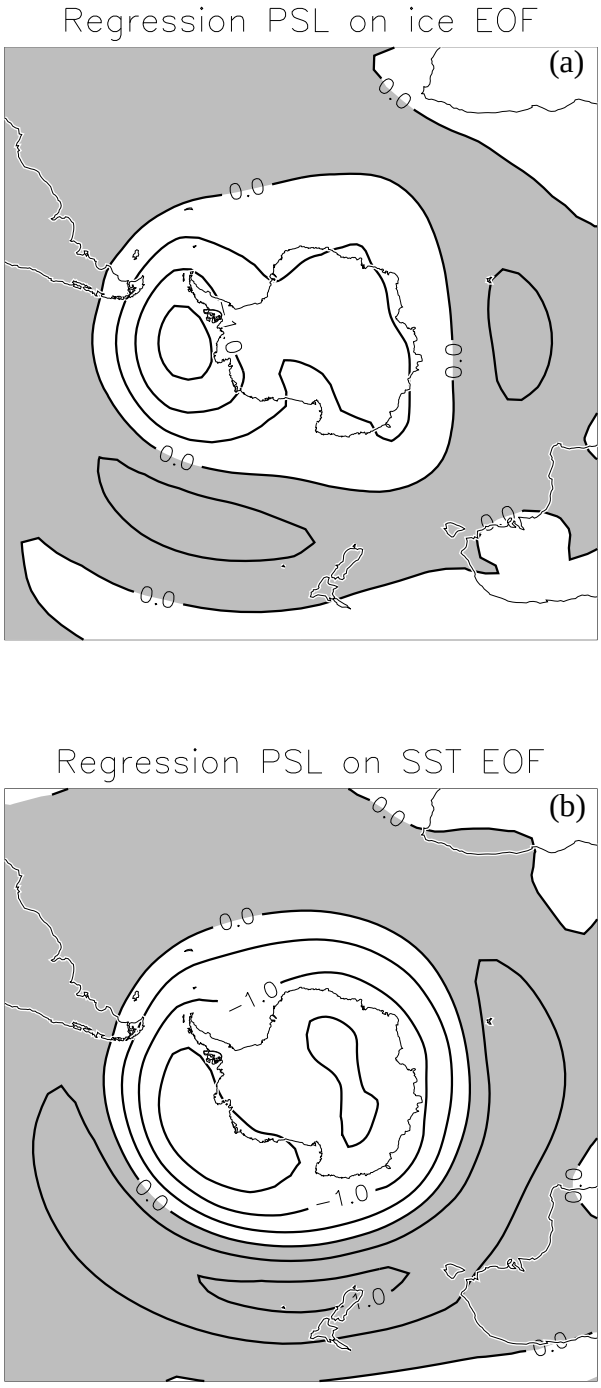

Figure 7. Annual averaged SLP regressed on the a) leading mode of sea ice variability and b) leading mode of SST variability. The contour interval is 0.5 mb per standard deviation of the principal component timeseries and positive values are shaded.

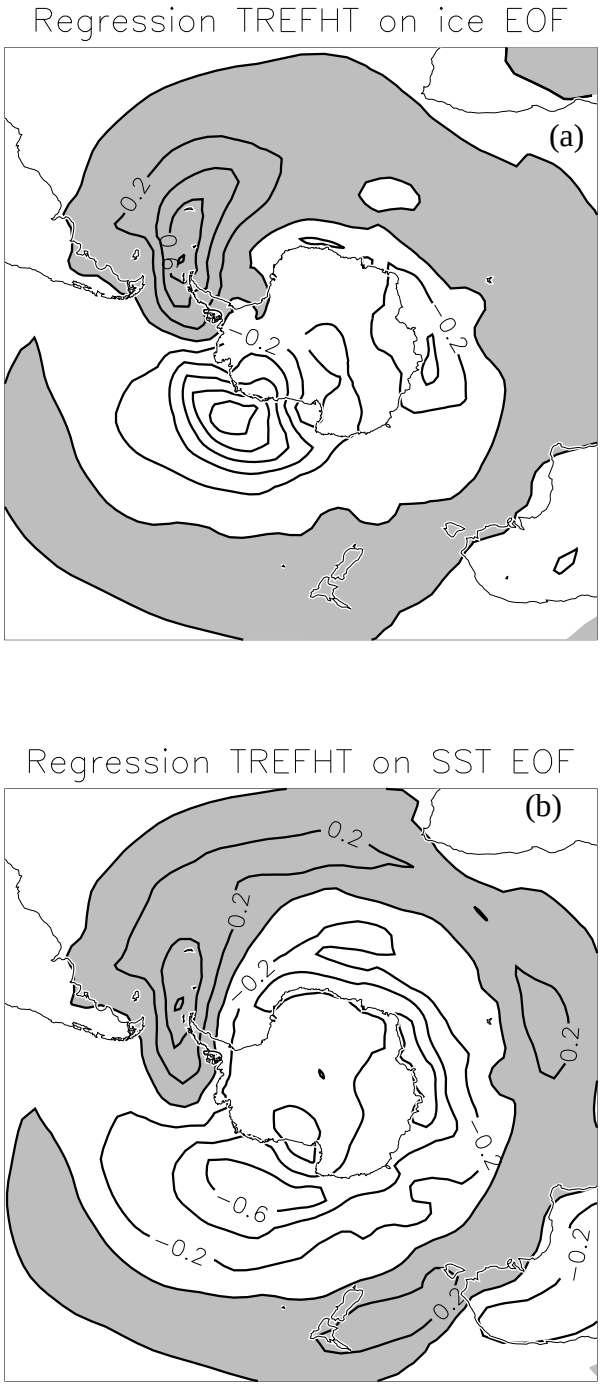

Figure 8. Annual averaged SAT regressed on the a) leading mode of sea ice variability and b) leading mode of SST variability. The contour interval is 0.2^{o}C per standard deviation of the principal component timeseries and positive values are shaded.

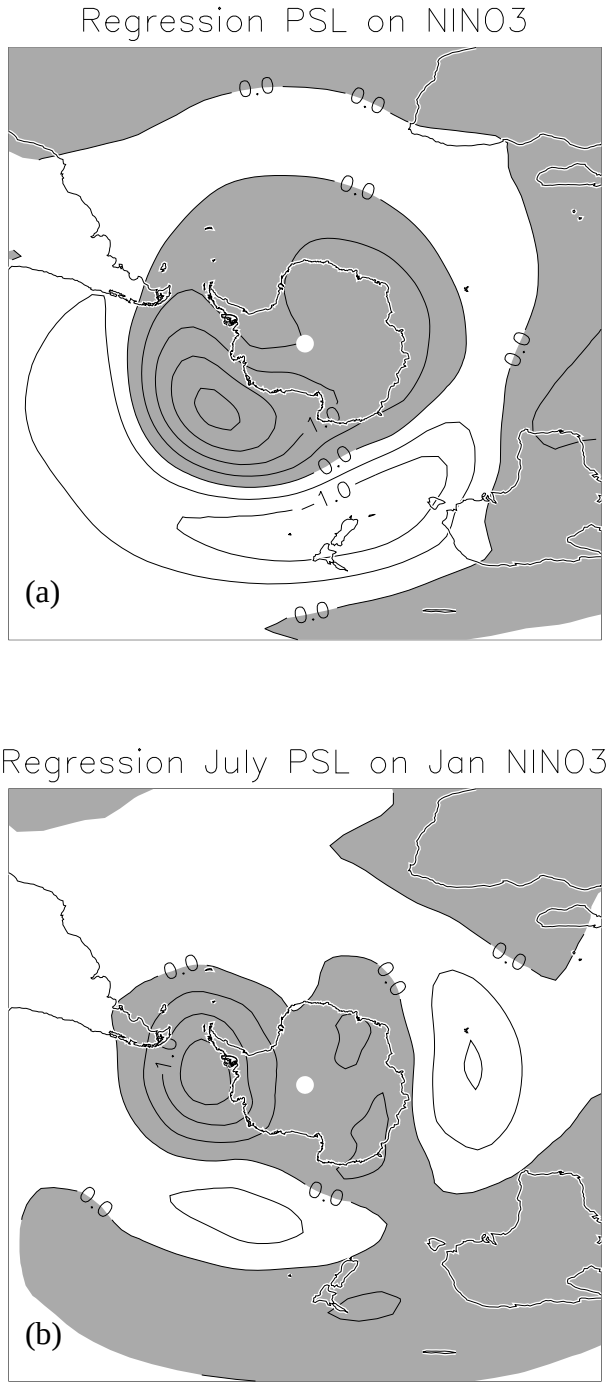

Figure 9. The (a) monthly SLP anomalies regressed on the monthly averaged NINO3 timeseries and (b) July SLP anomaly regressed on the previous January NINO3 timeseries. The contour interval is 0.5 mb per standard deviation of the NINO3 timeseries and positive values are shaded.

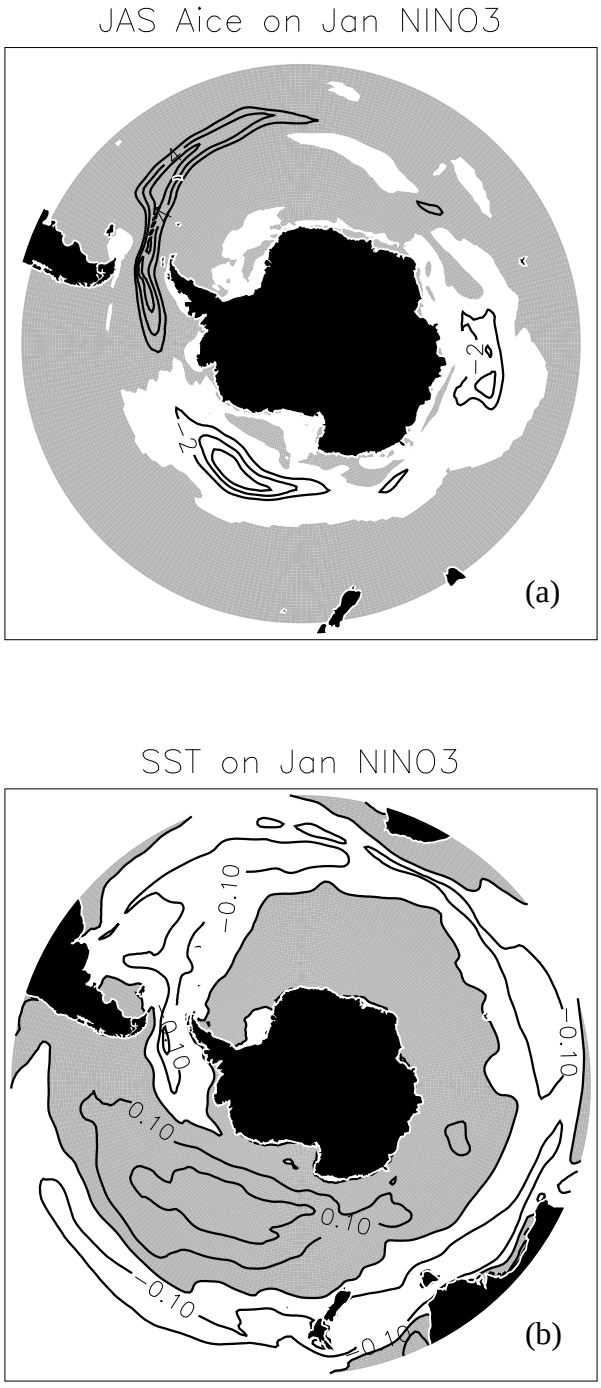

Figure 10. (a) JAS sea ice concentration and (b) annual averaged SST regressed on the January NINO3 timeseries. The contour interval is 2% fractional coverage per standard deviation of the NINO3 timeseries in (a) and 0.1^{o}C in (b) per standard deviation of the NINO3 timeseries. Positive values are shaded and the zero contour is not shown in (a).

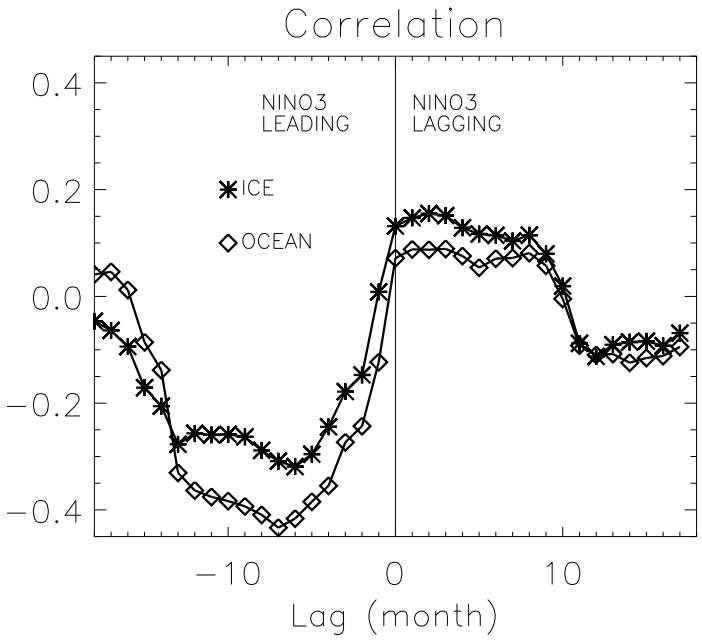

Figure 11. Correlation of the monthly NINO3 timeseries and the principal component of the leading mode of winter sea ice variability (*) and annual average SST variability (diamonds).

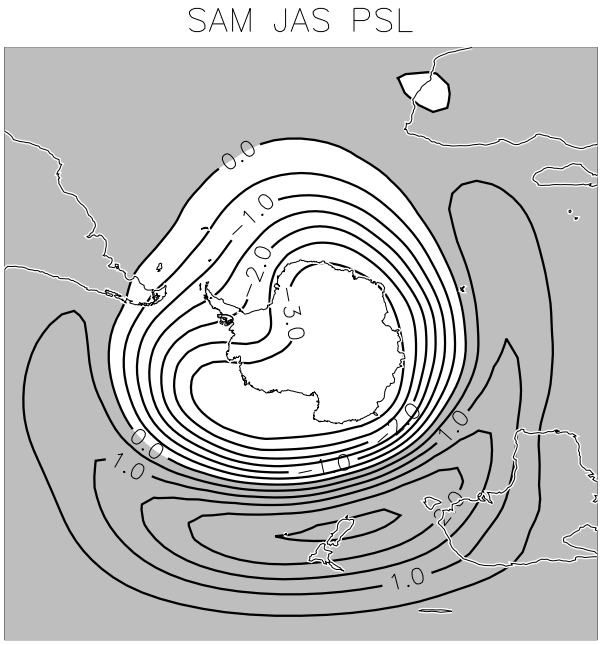

Figure 12. The first EOF of sea level pressure for the southern hemisphere from 20 to 90 S. The nondimensional EOF has been scaled by the standard deviation of the corresponding principal component timeseries to show the dimensional standard deviation of SLP at each grid point associated with the EOF. The contour interval is 0.5 mb and positive values are shaded.

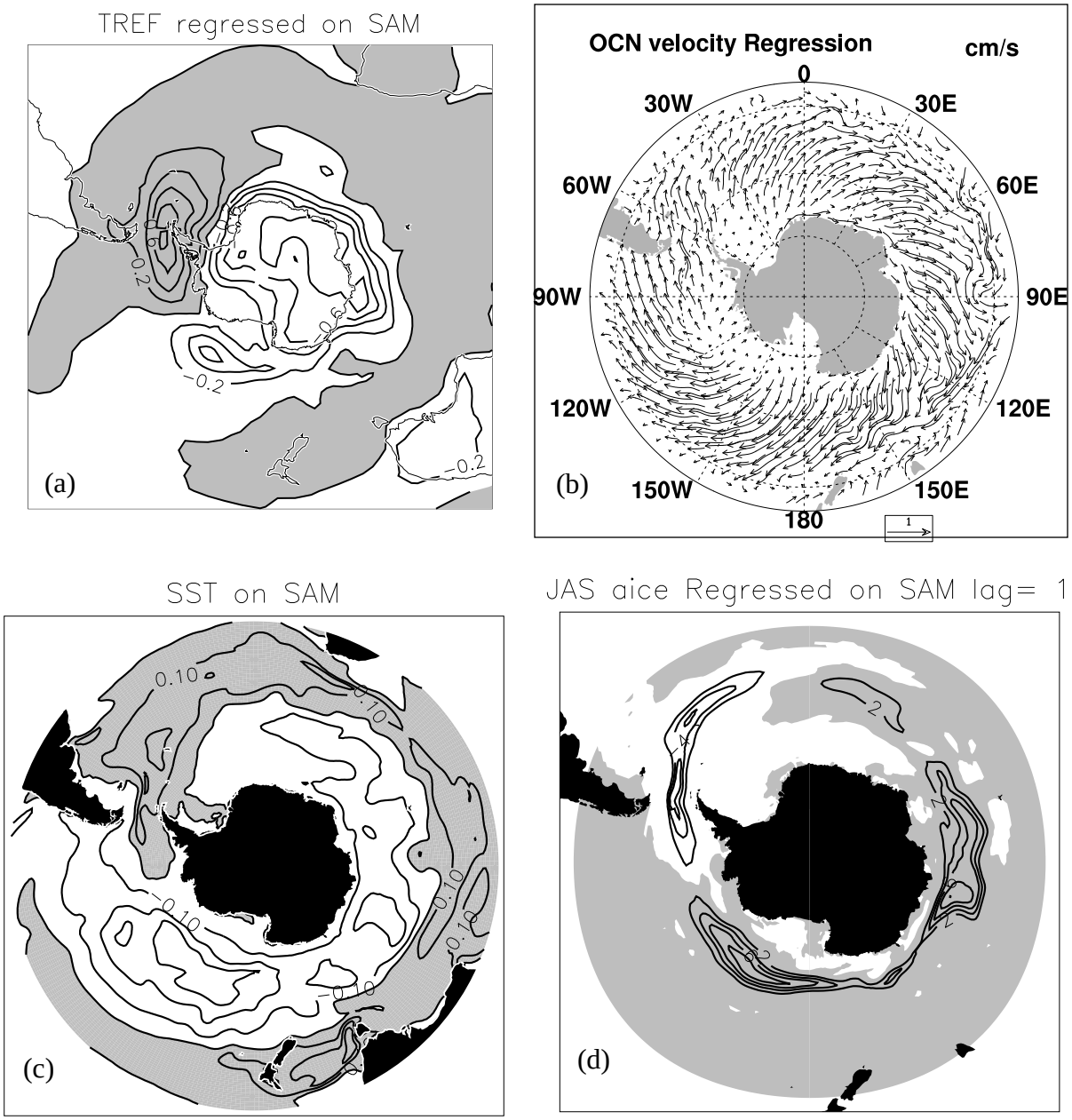

Figure 13. Climate variables associated with one standard deviation of the SAM index. Shown are a) SAT, with a contour interval of 0.2 oC, b) ocean surface velocity, c) SST, with a contour interval of 0.1 oC, and d) winter ice concentration lagged by one year, with a contour interval of 2% fractional coverage. Positive values are shaded and the zero contour interval is omitted from panel d.

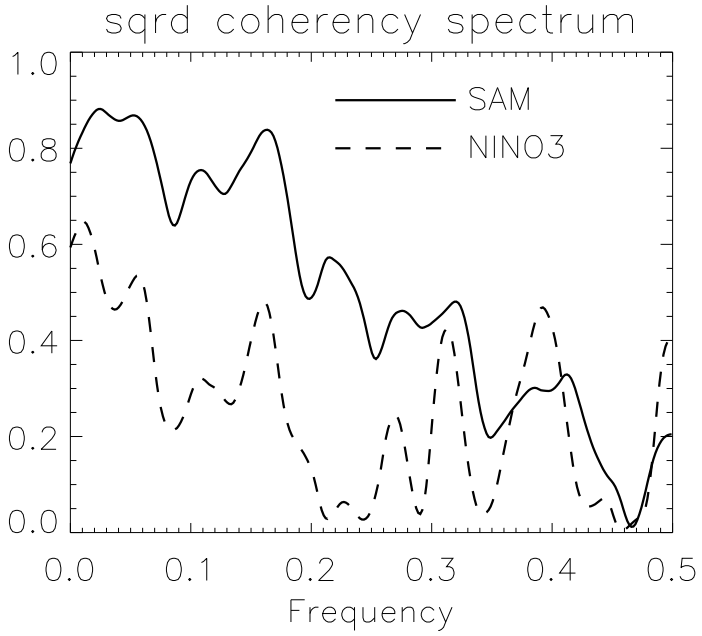

Figure 14. The squared coherency spectrum of the Antarctic sea ice Dipole and the SAM (solid line) and of the Antarctic sea ice Dipole and the January NINO3 timeseries (dashed line).